ECS Transactions, 80 (7) 203-216 (2017)
10.1149/08007.0203ecst ©The Electrochemical Society

(Invited)
Ultrawide Bandgap β-Ga_2O_3 Thin Films: Growths, Properties and Devices

Subrina Rafique, Lu Han, and Hongping Zhao*

Department of Electrical Engineering and Computer Science, Case Western Reserve University, Cleveland, Ohio 44106, USA
*Email: hongping.zhao@case.edu

Ultrawide bandgap β-Ga_2O_3 represents an emerging semiconducting material for high power electronics and short wavelength optoelectronics applications. It possesses a wide band gap of 4.5-4.9 eV, and excellent chemical and thermal stability up to 1400 ºC, which opens up new opportunities for various device applications. This paper reviews recent progresses on β-Ga_2O_3 thin film growths, properties and device demonstrations. Methods that have been demonstrated to enable high quality β-Ga_2O_3 thin film growth with controllable doping are discussed. Device applications of monoclinic β-Ga_2O_3 are also covered. Finally, a conclusion and future perspectives of the research in the area of this important semiconducting material will be given.

Introduction

Ultrawide bandgap (UWBG) semiconductor material gallium oxide (Ga_2O_3) has emerged as a new contender for next generation high power electronic devices and deep ultraviolet (DUV) solar blind photodetectors because of its unique material properties. Among the five known polymorphs (α, β, γ, δ, and ε), β phase Ga_2O_3 with monoclinic crystal structure represents the most thermally stable material. β-Ga_2O_3 has a room temperature bandgap of ~4.5-4.9 eV. It also possesses excellent chemical, mechanical and thermal stability at elevated temperatures. Due to its ultrawide bandgap that corresponds to the cut-off wavelength of ~250 nm, β-Ga_2O_3 is intrinsically solar-blind. As a result, DUV photodetectors based on β-Ga_2O_3 do not require any supplementary filter. It also avoids the alloying and thus simplifying the material growth process. Moreover, β-Ga_2O_3 based field effect transistors and diodes can have excellent power device characteristics such as high breakdown voltage, high power and low loss due to its very large bandgap. Based on the empirical relationship between the bandgap E_g and breakdown electric fields (E_{br}), the E_{br} of β-Ga_2O_3 is expected to have a value of about 6-8 MV/cm (1). The high E_{br} is the most attractive property of β-Ga_2O_3, because the Baliga's figure-of-merit (FOM), which is the basic parameter to evaluate how suitable a material is for power devices, is proportional to E_{br}^3, but is only linearly proportional to the mobility. As compared to SiC and GaN, the conduction loss of β-Ga_2O_3 power devices can be one order of magnitude lower at the same breakdown voltage. More advantageously, high quality β-Ga_2O_3 wafers can be synthesized in large volumes by scalable and low cost melt-growth techniques. This addresses the current commercial constraints of SiC and GaN based device technologies which lack affordable native substrates. Although scientific and technological research interest on β-Ga_2O_3 has greatly intensified recently, β-Ga_2O_3 thin

film growth is far from mature and the understanding of its fundamental material properties is still at infancy stage.

Basic Properties of β-Ga_2O_3

Crystal Structure of β-Ga_2O_3

Among all the polymorphs of gallium oxide, β-Ga_2O_3 has attracted the most attention because of its availability and outstanding properties. It is the only stable polymorph through the whole temperature range till melting point. β-Ga_2O_3 has a C-centered monoclinic unit cell with space group C2/m. The unit cell of β-Ga_2O_3 is shown in Fig. 1 (2). It contains two crystallographically inequivalent Ga positions, one with tetrahedral geometry Ga (I) and one with octahedral geometry Ga (II). Oxygen atoms have three crystallographically different positions and are denoted as O(I), O(II) and O(III), respectively. Two oxygen atoms are coordinated trigonally and one is coordinated tetrahedrally.

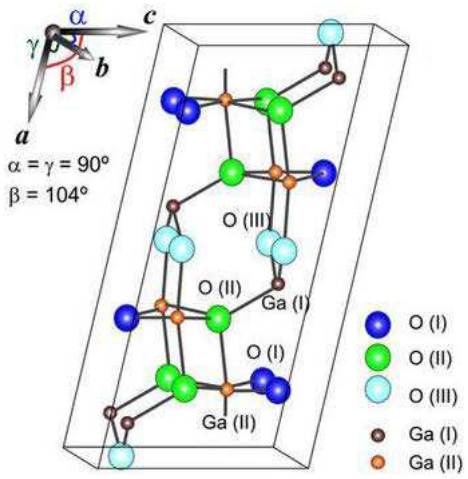

Figure 1: Unit cell of β-Ga_2O_3 (2).

Thermal Properties of β-Ga_2O_3

β-Ga_2O_3 has relative low thermal conductivities as compared to other semiconductors such as SiC, sapphire and GaN. Its thermal conductivity is about half of that of sapphire and one order of magnitude smaller than that of GaN (2). The thermal conductivity in β-Ga_2O_3 is highly dependent on its crystal direction due to the crystalline anisotropy. It was reported that at room temperature, the [010] direction had the highest thermal conductivity of 27 W/mK and the lowest thermal conductivity of 10.9 W/mK was along [100] direction (3). It was found that at low temperatures, the thermal conductivity of β-Ga_2O_3 does not exhibit the typical $T^{-3/2}$ dependence on temperature, indicating that heat conduction is limited not only by phonon scattering but also by free electron scattering (3, 4).

Growth of β-Ga_2O_3

β-Ga_2O_3 Bulk Growth

Large area single crystalline β-Ga_2O_3 substrates with excellent structural quality and controllable doping are indispensable for realizing practical device applications. Recently, renewed interest in Ga_2O_3 has arisen due to the successful growth of large area, single crystalline β-Ga_2O_3 substrates with excellent quality. High quality single crystalline β-Ga_2O_3 substrates have been synthesized by melt based methods including the edge-defined film-fed growth (EFG) (5, 6), floating zone (7-12) and Czochralski (13-16) methods. The substrates obtained through these methods are expected to be scalable and low cost (17). The as-grown β-Ga_2O_3 substrates exhibit n-type conductivity which is believed to be due to the Si impurity from the Ga_2O_3 powder source. Semi-insulating Ga_2O_3 substrates can be achieved by using Fe, Mg dopants (18, 19).

β-Ga_2O_3 Thin Film Growth

β-Ga_2O_3 thin films have been grown by various methods including molecular beam epitaxy (MBE) (20-24), metal organic vapor phase epitaxy (MOVPE) (25-28), halide vapor phase epitaxy (HVPE) (29-31), and low pressure chemical vapor deposition (LPCVD) (32-34).

β-Ga_2O_3 MBE Growth

MBE is a well known technique to produce high quality thin films with reduced impurity level. It can grow thin films with lower unintentional impurity levels due to an ultrahigh vacuum environment and high purity source materials. Typically, MBE growth of β-Ga_2O_3 thin films is carried out in the temperature range between 550 ºC-800 ºC using high purity gallium (Ga) source. For oxygen source, both O_2 (20, 21, 23, 24) and O_3 (22) are being used. The growth rates of the MBE grown β-Ga_2O_3 thin films are in the range between 50 -180 nm/hr. The limited growth rate is due to the growth kinetics associated with the technique. Current efforts for doped β-Ga_2O_3 thin films growth by MBE involves the use of Sn and Ge as N-type dopant sources (22, 35, 36). By using Sn, the carrier concentration was tuned in the range between 10^{16}-10^{19} cm^{-3} (22); whereas the carrier concentration was tuned in the range between 10^{18}-10^{19} cm^{-3} using Ge (36). The maximum achievable mobility so far using Sn and Ge were ~150 $cm^2/V.s$ and 97 $cm^2/V.s$, respectively.

β-Ga_2O_3 MOVPE Growth

MOVPE is a commercial technique to produce high quality III-V and III-nitride epitaxy. It can grow high volume material with conformal deposition. MOVPE growth of β-Ga_2O_3 thin films is carried out in the temperature range between 550 ºC-850 ºC Triethylgallium (TEGa), Trimethylgallium (TMGa) and high purity O_2 are used as the sources. The growth rates of the MOVPE grown thin films typically vary in the range between 120 -750 nm/hr. For N-type doping of β-Ga_2O_3 thin films grown by MOVPE, both Si and Sn are used as dopants (28, 37, 38). However, N-type doping of Ga_2O_3 thin films using MOVPE is not trivial. When using Sn as an N-type dopant, it leaves

pronounce memory effect inside the growth chamber. As a result, it is hard to grow a thin film with low doping concentration after high dopant flow growth. Sn also forms different complexes and extended defects in the thin films which in turns degrades the material quality. In case of Si, it forms SiO_2 because of the large affinity of Si to oxygen. As a result, Si dopants are passivated and not electrically active. The highest reported mobility so far was 130 $cm^2/V.s$ for a Si doped thin film having a carrier concentration of ~$1x10^{17}$ cm^{-3} (28).

β-Ga_2O_3 HVPE Growth

HVPE is a cost effective growth technique developed in Japan that can produce materials with good crystalline quality and faster growth rate. HVPE growth of β-Ga_2O_3 thin films is carried out at ~1050 ºC using Gallium chloride (GaCl) and O_2 as precursors. N_2 is used as the carrier Gas. The fastest growth rate reported to date was ~25 µm/hr for the β-Ga_2O_3 homoepitaxial layer on (001) substrate (30). For N-type doping of HVPE grown β-Ga_2O_3 thin films, silicon tetrachloride ($SiCl_4$) is used as an efficient dopant source. Due to the fast growth rate, the thin films suffer from surface roughness. As result, additional polishing procedure is required prior device processing. Also because of the use of GaCl as the Ga source, the thin films show the presence of Cl induced impurity and defect.

β-Ga_2O_3 LPCVD Growth

LPCVD is a scalable and low cost technique that can produce high quality material with faster growth rate, controllable doping and high mobility (32-34). LPCVD growth of β-Ga_2O_3 thin films is carried out in the temperature range between 780 ºC-950 ºC using high purity metallic Ga and O_2 gas as the source materials. $SiCl_4$ is used as N-type dopant. Controllable growth rates of β-Ga_2O_3 thin films ranging between 0.5-10 µm/h have been achieved via LPCVD growth method by tuning the growth parameters such as growth temperature, growth pressure and precursor flow rate. Figure 1(a) shows the top view FESEM image of a heteroepitaxial unintentionally doped (UID) β-Ga_2O_3 thin film grown for 2 h on a c-plane sapphire substrate at 800 ºC. The thin film is composed of small domains having pseudo hexagonal morphology. The cross-sectional FESEM image of the β-Ga_2O_3 thin film shown in Figure 1(b) was obtained from the same sample. The thin film has a thickness of 3.42 µm. This corresponds to a growth rate of 1.7 µm/h for this film. The crystal quality of the thin film was characterized by X-ray diffraction (XRD) rocking curve measurement. Figure 2 shows the XRD rocking curve of the (-201) diffraction peak of the same β-Ga_2O_3 thin film. The full width at half maximum (FWHM) of the rocking curve is measured as 1.494º. Optical properties of the as-grown thin films were characterized by room temperature absorbance spectrum. Figure 3 shows the absorbance spectrum of the Ga_2O_3 thin film grown at 900 ºC. The thin film has a strong absorption in the deep UV region with a sharp absorption edge at around 260 nm. The estimated optical bandgaps obtained from the Tauc plot is E_g - 4.76 eV, as shown in the inset of Fig. 3.

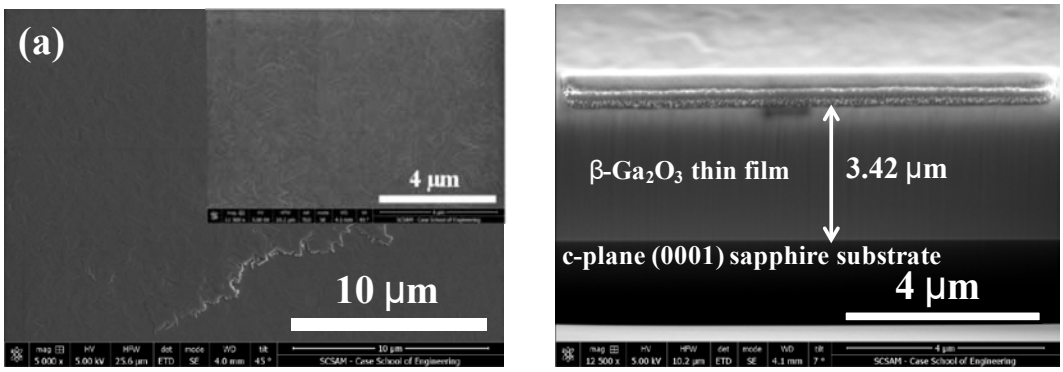

Figure 1. (a) Top view FESEM image of as-grown UID β-Ga_2O_3 thin film grown on c-plane sapphire substrate. Inset shows the high magnification top view of the FESEM image. (b) Cross sectional FESEM image of UID β-Ga_2O_3 thin film. Layer thickness is ~3.42 µm (34).

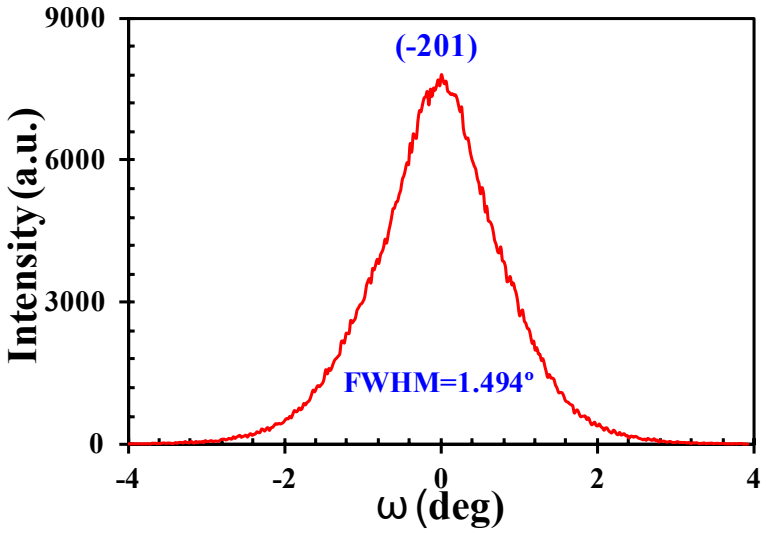

Figure 2. XRD rocking curve of (-201) reflection of β-Ga_2O_3 thin film (34).

The electrical properties of the LPCVD grown heteroepitaxial β-Ga_2O_3 thin films represent the best quality among the reported ones. Figure 4 plots the Hall mobility as a function of the n-type carrier concentration for the as grown Si-doped β-Ga_2O_3 thin films grown by LPCVD. By varying the doping source flow rate, the carrier concentration can be widely tuned between high-10^{16} to high-10^{19} cm^{-3} range. The measured room temperature Hall mobility ranged between 8- 42.35 $cm^2/V.s$. With further optimization of the growth condition, electron Hall mobility can reach >100 $cm^2/V.s$ with a doping concentration in the low-10^{18} cm^{-3}.

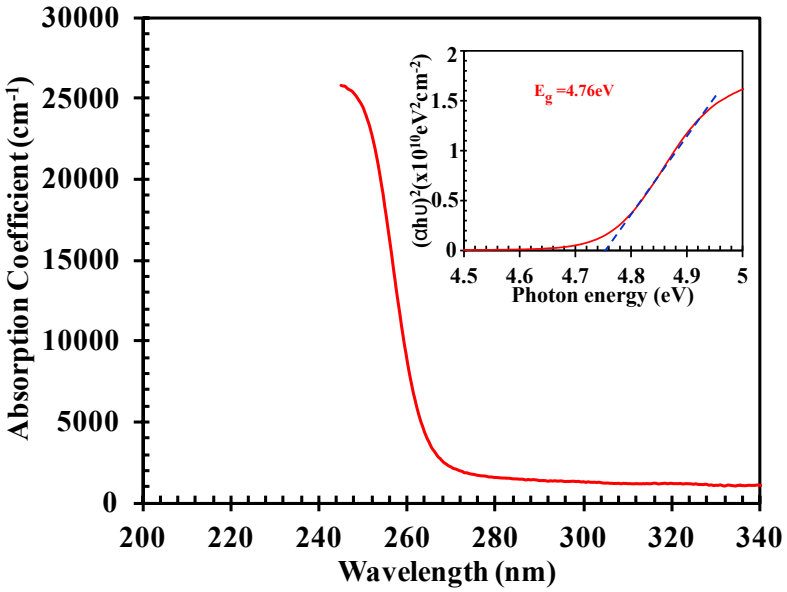

Figure 3. Room temperature absorbance spectrum β-Ga_2O_3 thin film grown on c-plane sapphire substrate grown at 900 °C. The inset shows the Tauc plot of $(\alpha h\upsilon)^2$ versus photon energy (hυ) for the thin film. (34).

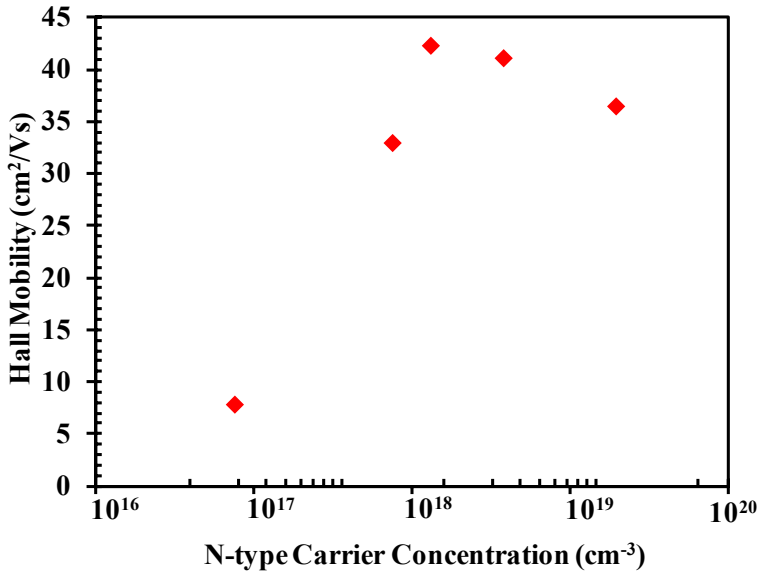

Figure 4. Electron Hall mobility as a function of carrier concentration for the LPCVD grown Si-doped β-Ga_2O_3 thin film on c-plane sapphire substrate (34).

Homoepitaxial growth of β-Ga_2O_3 thin films on (010) β-Ga_2O_3 substrates had also been reported by LPCVD. Figure 5 shows the cross sectional FESEM image of the β-Ga_2O_3 TEM sample, which was grown at 850 °C for 40 min. From this image, the thickness of the homoepitaxial layer was estimated to be 0.86 μm, which corresponded to a growth rate of 1.3 μm/h. By tuning the growth conditions, similar growth rate for the homoepitaxial thin films can be achieved as the heteroepitaxial ones.

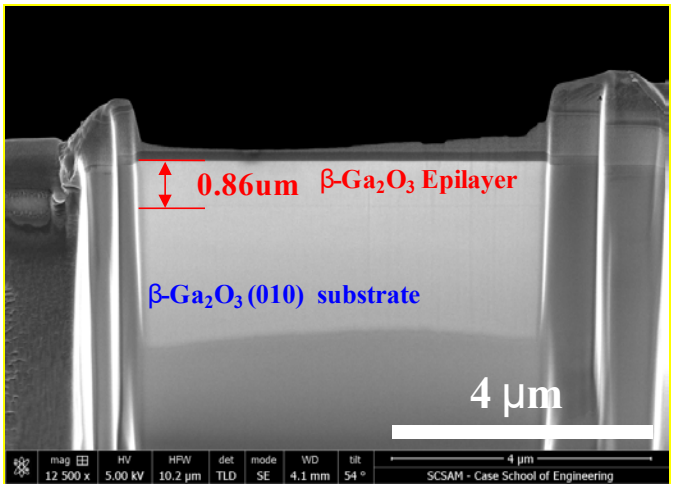

Figure 5. Cross sectional FESEM image of TEM sample prepared by FIB from a homoepitaxial β-Ga_2O_3 thin film (33).

The crystal quality of the homoepitaxial thin film was characterized by XRD rocking curve. Figure 6 shows the XRD rocking curves of (-42-2) reflection of β-Ga_2O_3 homoepitaxial layer synthesized at growth temperature of 900 ºC and 950 ºC. The XRD rocking curve full width at half maximum (FWHM) of (-42-2) peak for the layer grown at 900 ºC and the substrate were 40 and 20 arc sec, respectively. The small value of the FWHM of the homoepitaxial layer demonstrates a high quality epitaxial film with very low dislocations and strain.

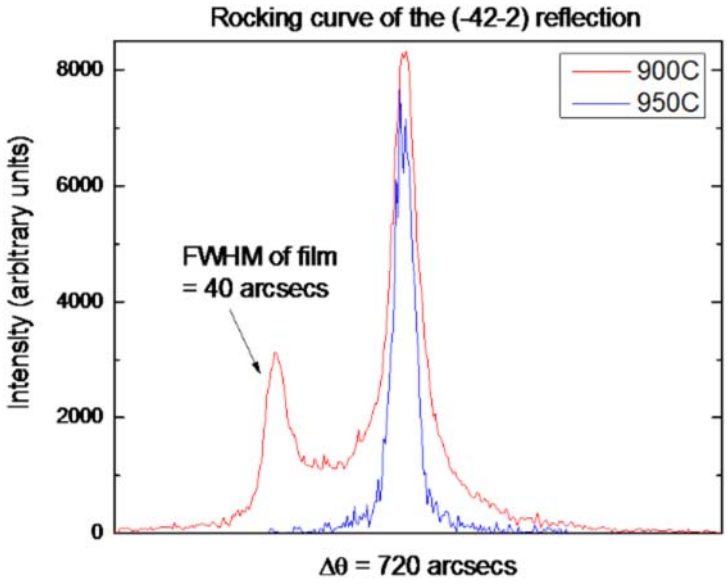

Figure 6. XRD rocking curves of (-42-2) reflection peak of β-Ga_2O_3 homoepitaxial layer grown at 900 ºC and 950 ºC (33).

Note that there have been no reports so far on achieving conductive Ga_2O_3 material with p type dopant due to the predicted large ionization energies, presence of n-type impurities and native defects (1). This requires a systematic investigation of the ionization energies of candidate acceptors and a better understanding of the compensation by native point defects. The understanding of native defects in Ga_2O_3 is far from complete and has been largely driven by first principal calculations using different approaches (39).

β-Ga_2O_3 Devices

β-Ga_2O_3 Processing

Etching is necessary for intra-device isolation or for exposing layers for subsequent contacting. Studies need to be conducted to understand properly the wet and dry etching characteristics of β-Ga_2O_3 and the associated mechanisms and effects on the properties of the material. High quality contacts are a prerequisite for any device and need to provide low contact resistance at moderate annealing temperatures. Many published I-V characteristics for β-Ga_2O_3 based devices are only quasi-linear at low current and shows the need for improved contact approaches that exist for the more mature semiconductors.

The choice of gate dielectric for any semiconductor material depends on three criteria: (i) it must be thermodynamically stable with the semiconductor and not react during processing; (ii) it should have a high quality interface with low defect and trap density; and (iii) it must have sufficient band offsets to act as both electron and hole barriers. The device performance depends largely on the band offsets and type of band alignment. The ultra-wide bandgap of β-Ga_2O_3 limits the available choices of gate dielectrics to those with bandgaps > 6 eV such as SiO_2, Al_2O_3, $HfSiO_4$, Y_2O_3, La_2O_3, HfO_2, ZrO_2 and $LaAlO_3$ (40-43). Measurements of band offsets of different dielectrics with β-Ga_2O_3 are at their early stage. Further optimization of the etch conditions for patterning the dielectrics and improving their interface quality with β-Ga_2O_3 is still needed.

β-Ga_2O_3 based power devices will need thermal management because of the limited and anisotropic thermal conductivity of the material. This issue might be addressed using heat sinks like diamond or microfluidic approaches or by transferring to a metal substrate. These approached are currently being developed for GaN power electronics. However, the lower thermal conductivity of β-Ga_2O_3 relative to other wide bandgap materials means these techniques need to be more effective in order to utilize β-Ga_2O_3 in high-power devices.

β-Ga_2O_3 Field Effect Transistors

β-Ga_2O_3 based field effect transistors (FETs) have been recently studied because of their promising applications as next generation power electronics. FETs based on both β-Ga_2O_3 single crystal and thin films grown by MBE and MOVPE have been demonstrated (44-48). FETs fabricated on thin flakes and nanomembranes exfoliated mechanically from bulk β-Ga_2O_3 single crystals have also been reported by several groups (49-51). The highest reported breakdown voltage achieved so far for β-Ga_2O_3 thin film based FET is 3.8 MV/cm (45), surpassing theoretical bulk critical field strengths for GaN (3.3 MV/cm) and SiC (2.5 MV/cm) (45).

β-Ga_2O_3 Schottky Barrier Diodes

Due to its predicted high breakdown electric field (E_b ~ 6-8 MV/cm) and reasonable electron mobility (μ ~ 200-300 cm^2/Vs), β-Ga_2O_3 is expected to have much larger Baliga's figure of merit (FOM) ($\varepsilon\mu E_b^3$, where ε is relative dielectric constant) as compared to SiC or GaN. β-Ga_2O_3 based Schottky barrier diodes (SBDs) with reasonably good device characteristics have been demonstrated (52-56). The highest reported breakdown voltage achieved so far is ~1076 V for a β-Ga_2O_3 drift layer based field-plated (FP) SBD grown by HVPE (56).

β-Ga_2O_3 Photodetectors

Deep-ultraviolet (DUV) solar-blind (cut-off wavelength<280 nm) photodetectors (PDs) have received considerable research attentions due to their applications in both military and civil surveillance such as missile tracking, secure communication, ozone hole monitoring, flame detection and chemical/biological analysis. Monoclinic β-Ga_2O_3 is a promising candidate for DUV PD because of its desirable properties such as bandgap of ~4.5-4.9 eV and excellent chemical, mechanical and thermal stability. As a result, many studies on β-Ga_2O_3 based solar-blind PDs have appeared in recent years. β-Ga_2O_3 nanomaterials (57, 58), thin films (59-62) and single crystals (63-65) have been used as the active layers for such PDs. However, effects of interband defect levels on the PD device performance are still not well understood yet.

Ga_2O_3 Gas Sensors

Many Ga_2O_3 based gas sensors using thin films and nanomaterials have been investigated recently (66-73). Oxygen sensors function based on the fact that the conductivity of β-Ga_2O_3 thin films is inversely proportional to the oxygen partial pressure in the surrounding ambient. At temperatures around 600 ºC, the oxygen sensitivity of Ga_2O_3 reduces significantly and it can instead be used to detect reducing gases such as hydrogen. The H_2 induced changes in the electrical conductance of Ga_2O_3 result from reversible chemisorption of the hydrogen on the whole surface of the Ga_2O_3 with subsequent electron transfer from the adsorbed hydrogen to the Ga_2O_3. However, it should be pointed out that the response of Ga_2O_3 sensor towards reducing components like ethanol or propane cannot be neglected in comparison with the oxygen response even at high temperature of 800 ºC (74). The cross-sensitivity to reducing components can be suppressed by additional catalytic or filter layers (74).

Ga_2O_3 Photocatalysis

Photocatalytic systems using solar energy have attracted much attention due to their potential for alleviation of the environmental energy problems. Ga_2O_3 is one of the attractive photocatalyst materials because it has shown high photocatalytic activities for various reactions such as water splitting (75), reduction of carbon dioxide (76, 77), conversion of methane (78, 79) and decomposition of organic compounds (80). The catalytic activity of Ga_2O_3 is attributed to the unique structural characteristics of

coordinatively unsaturated surface Ga^{3+} cations, which is believed to be crucial for hydrocarbon activation in CO_2 atmosphere (77).

β-Ga_2O_3 Substrates for III-nitrides Epitaxy

Native GaN substrates are costly and difficult to obtain despite the recent progress in bulk GaN single crystal synthesis. For that reason, the majority of gallium nitride devices are produced by heteroepitaxial growth on foreign substrates such as sapphire, silicon or silicon carbide. However, challenges still exist with these materials such as insulating nature of sapphire makes it impossible to produce vertical devices. In case of SiC, it is expensive and has high optical absorption in the blue region of the spectrum. Silicon also has many disadvantages such as large thermal and lattice mismatch, chemical interaction with GaN in the growth environment and opaqueness in visible and UV spectra. Monoclinic β-Ga_2O_3 is a good candidate serving as a growth substrate for III-nitrides, as it combines the advantages of transparent and conductive substrate. More advantageously, high quality bulk β-Ga_2O_3 crystals can be produced by melt-growth techniques such as Czochralski and EFG at low cost and high throughput. As a result, there are several reports published recently on the synthesis of GaN epilayers on different orientations of β-Ga_2O_3 substrates by MOVPE (78-80), MBE (81,82) and HVPE (78).

Conclusion

This paper provides a brief overview of the current status of research to date in the study of β-Ga_2O_3 as a potential candidate for various applications. Significant progresses have been made recently in bulk and thin film growth, defect and impurity control, doping and etc. Proof of concept prototypes of β-Ga_2O_3 transistors and Schottky diodes have been demonstrated. Despite the fact that a significant progress has been made, β-Ga_2O_3 research and development is still far from being mature. There are still important issues that need to be explored for realization of full potential of β-Ga_2O_3 material for practical device applications. Understanding of the fundamental defects in the as-grown β-Ga_2O_3 thin films are still lacking. Moreover, it is of fundamental importance to understand the effect of various growth parameters on the optical, structural and electrical properties of β-Ga_2O_3 thin films. The fabrication of high quality devices based on β-Ga_2O_3 thin films is an area of research that should be pursued further in the future.

References

1. K. Sasaki, M. Higashiwaki, A. Kuramata, T. Masui, and S. Yamakoshi, *J. Cryst. Growth,* **378**, 591 (2013).
2. S. I. Stepanov, V. I. Nikolaev, V. E. Bougrov, and A. E. Romanov, *Rev. Adv. Mater.,* **44**, 63 (2016).
3. Z. Guo, A. Verma, X. Wu, F. Sun, A. Hickman, T. Masui, A. Kuramata, M. Higashiwaki, D. Jena, and T. Luo, *Appl. Phys. Lett.,* **106**, 111909 (2015).

4. Z. Galazka, K. Irmscher, R. Uecker, R. Bertram, M. Pietsch, A. Kwasniewski, M. Naumann, T. Schulz, R. Schewski, D. Klimm, and M. Bickermann, *J. Cryst. Growth,* **404**, 184 (2014).
5. H. Aida, K. Nishiguchi, H. Takeda, N. Aota, K. Sunakawa, and Y. Yaguchi, Jpn. *J. Appl. Phys.,* **47**, 8506 (2008).
6. T. Oishi, Y. Koga, K. Harada, and M. Kasu, *Appl. Phys. Expres,s* **8**, 031101 (2015).
7. Y. Tomm, J. M. Ko, A. Yoshikawa, and T. Fukuda, *Sol. Energy Mater. Sol. Cells,* **66**, 369 (2001).
8. E. G. Villora, K. Shimamura, Y. Yoshikawa, K. Aoki, and N. Ichinose, *J. Cryst. Growth,* **270**, 420 (2004).
9. J. Zhang, B. Li, C. Xia, G. Pei, Q. Deng, Z. Yang, W. Xu, H. Shi, F. Wu, Y. Wu, and J. Xu, J. *Phys. Chem. Solids*, **67**, 2448 (2006).
10. S. Ohira, N. Suzuki, N. Arai, M. Tanaka, T. Sugawara, K. nakajima, and T. Shishido, *Thin Solid Films,* **516**, 5763 (2008).
11. E. G. Villora, K. Shimamura, Y. Yoshikawa, T. Ujiie, and K. Aoki, *Appl. Phys. Lett.,* **92**, 202120 (2008).
12. T. C. Lovejoy, E. N. Yitamben, N. Shamir, J. Morales, E. G. Villora, K. Shimamura, S. Zheng, F. S. Ohuchi, and M. A. Olmstead, *Appl. Phys. Lett.,* **94**, 081906 (2009).
13. Z. Galazka, R. Uecker, K. Irmscher, M. Albrecht, D. Klimm, M. Pietsch, M. Brutzam, R. Bertram, S. Ganschow, and R. Fornari, *Cryst. Res. Techmol.*, **45**, 1229 (2010).
14. K. Irmscher, Z. Galazka, M. Pietsch, R. Uecker, and R. Fornari, *J. Appl. Phys.*, **110**, 063720 (2011).
15. Z. Galazka, K. Irmscher, R. Uecker, M. Albrecht, R. Bertram, M. Pietsch, A. Kwasneiwski, M. Naumann, T. Schulaz, R. Schewski, D. Klimm, and M. Bickermann, *J. Cryst. Growth,* **404**, 184 (2014).
16. M. Handwerg, R. Mitdank, Z. Galazka, and S. F. Fischer, *Semicond. Sci. Technol.,* **30**, 024006 (2015).
17. M. Higashiwaki, K. Sasaki, A. Kuramata, T. Masui, and S. Yamakoshi, *Phys. Status Solidi A,* **211**, 21 (2014).
18. M. Slomski, N. Blumenschein, P. P. Paskov, J. F. Muth, and T. Paskova, *J. Appl. Phys.,* **121**, 235104 (2017).
19. T. Harwig, G. J. Wubs, and G. J. Dirksen, *Solid State Commun.,* **18**, 1223 (1976).
20. E. G. Villora, K. Shimamura, K. Kitamura, and K. Aoki, *Appl. Phys. Lett.,* **88**, 031105 (2006).
21. K. Sasaki, A.Kuramata, T. Masui, E. G. Villora, K. Shimamura, and S. Yamakoshi, *Appl. Phys. Express,* **5**, 035502 (2012).
22. K. Sasaki, A. Kuramata, T. Masui, E. G. Villora, K. Shimamura, and S. Yamakoshi, *Appl. Phys. Express,* **5**, 035502 (2012).
23. K. Sasaki, M. Higashiwaki, A. Kuramata, T. Masui, and S. Yamakoshi, *J. Cryst. Growth,* **392**, 30 (2014).
24. D. Guo, Z. Wu, P. Li, Y. An, H. Liu, X. Guo, H. Yan, G. Wang, C. Sun, L. LI, and W. tang, *Opt. Mater. Express*, **4**, 1067 (2014).
25. N. H. Kim, H. W. Kim, C. Seoul, and C. Lee, *Mater. Sci. Eng. B,* **111**, 131 (2004).
26. H. W. Kim, and N. H. Kim, *Mater. Sci. Eng.,* **110**, 34 (2004).

27. G. Wagner, M. Baldini, D. Gogova, M. Schmidbauer, R. Schewski, M. Albrecht, Z. Galazka, D. Klimm, and R. Fornari, *Phys Status Solidi A,* **211**, 27 (2014).
28. M. Baldini, M. Albrecht, A. Fiedler, K. Irmscher, R. Schewski, and G. Wagner, *ECS J. Solid State Sci. Technol.,* **6**, Q3040 (2017).
29. K. Nomura, K. Goto, R. Togashi, H. Murakami, Y. Kumagai, A. Kuramata, S. Yamakoshi, and A. Koukitu, *J. Cryst. Growth*, **405**, 19 (2014).
30. H. Murakami, K. Nomura, K. Goto, K. Sasaki, K. Kawara, Q. T. Thieu, R. Togashi, Y. Kumagai, M. Higashiwaki, A. Kuramata, S. Yamakoshi, B. Monemar, and A. Koukitu, *Appl. Phys. Express*, **8**, 015503 (2015).
31. V. I. Nikolaev, A. I. Pechnikov, S. I. Stepanov, I. P. Nikitina, A. N. Smirnov, A. V. Chikiryaka, S. S. Sharofidinov, V. E. Bougrov, and A. E. Romanov, *Mater. Sci. Semicond. Process.,* **47**, 16 (2016).
32. S. Rafique, L. Han, and H. Zhao, *Phys. Status Solidi A*, **213**, 1002 (2016).
33. S. Rafique, L. Han, M. J. Tadjer, J. A. Freitas Jr., N. A. Mahadik, and H. Zhao, *Appl. Phys. Lett.*, **108**, 182105 (2016).
34. S. Rafique, L. Han, A. T. Neal, S. Mou, M. J. Tadjer, R. H. French, and H. Zhao, *Appl. Phys. Lett.*, **109**, 132103 (2016).
35. H. Okumura, M. Kita, K. Sasaki, A. Kuramata, M. Higashiwaki, and J. S. Speck, *Appl. Phys. Express,* **7**, 095501 (2014).
36. E. Ahmadi, O. S. Koksaldi, S. W. Kaun, Y. Oshima, D. B. Short, U. K. Mishra, J. S. Speck. *Appl. Phys. Express,* **10**, 041102 (2017).
37. M. Baldini, M. Albrecht, A. Fiedler , K. Irmscher , D. Klimm, R. Schewski , and G. Wagner, *J. Mater. Sci.,* **51**, 3650 (2016).
38. X. Du, Z. Li, C. Luan, W. Wang, M. Wang, X. Feng, H. Xiao, and J. Ma, *J. Mater. Sci.,* **50**, 3252 (2015).
39. M. Mohamed, C. Janowitz, I. Unger, R. Manzke, Z. Galazka, R. Uecker, R. Fornari, J. R. Weber, J. B. Varley, and C. G. Van De Walle, *Appl. Phys. Lett.,* **97**, 211903 (2010).
40. T. Kamimura, K. Sasaki, M. H. Wong, D. Krishnamurthy, A. Kuramata, T. Masui, S. Yamakoshi, and M. Higashiwaki, *Appl. Phys. Lett*., **104**, 192104 (2014).
41. V. D. Wheeler, D. I. Shahin, M. J. Tadjer, and C.R. Eddy Jr., *ECS J. Solid State Sci. Technol*., **6**, Q3052 (2017).
42. Y. Jia, K. Zeng, J. S. Wallace, J. A. Gardella, and U. Singisetti, *Appl. Phys. Lett*., **106**, 102107 (2015).
43. M. J. Tadjer, N. A. Mahadik, V. D. Wheeler, E. R. Glaser, L. Ruppalt, A. D. Koehler, K. D. Hobart, C. R. Eddy Jr., and F. J. Kub, *ECS J. Solid State Sci. Technol*., **5**, P468 (2016).
44. M. Higashiwaki, K. Sasaki, A. Kuramata, T. Masui, and S. yamakoshi, Appl. Phys. Lett. **100**, 013504 (2012).
45. A. J. Green, K. D. Chabak, E. R. Heller, R.C. Fitch, M. Baldini, A. Fiedler, K. Irmscher, G. Wagner, Z. Galazka, S. E. Tetlak, A. Crespo, K. Leedy, and G. H. Jessen, *IEEE Electron Device Lett.,* **37**, 902 (2016).
46. K. Zeng, J. S. Wallace, C. Heimburger, K. Sasaki, A. Kuramata, T. Masui, J. A. Gardella Jr., and U. Singisetti, *IEEE Electron Device Lett.,* **38**, 513 (2017).
47. M. J. Tadjer, N.A. Mahadik, V. D. Wheeler, E. R. Glaser, L. Ruppalt, A. D. Koehler, K. D. Hobart, C. R. Eddy, Jr., and F. J. Kub, *ECS J. Solid State Sci. Technol.,* **5**, P468 (2016).

48. M. H. Wong, K. Sasaki, A. Kuramata, S. Yamakoshi, and M. Higashiwaki, *IEEE Electron Device Lett.,* **37**, 212 (2016).
49. S. Ahn, F. Ren, J. Kim, S. Oh, J.Kim, M. A. Mastro, and S. J. Pearton, *Appl. Phys. Lett.,* **109**, 062102 (2016).
50. W. S. Hwang, A. Verma, H. Peelaers, V. Protasenko, S. Rouvimov, H.Xing, A. Seabaugh, W. Haensch, C.Van de Walle, Z. Galazka, M. Albrecht, R. Fornari, and D. Jena, *Appl. Phys. Lett.,* **104**, 203111 (2014).
51. H. Zhou, M. Si, S. Alghamdi, G. Qiu, L. Yang, and P. D. Ye, *IEEE Electron Device Lett.,* **38**, 103 (2017).
52. M. Mohamed, K. Irmscher, C. Janowitz, Z. Galazka, R. Manzke, and R. Fornari, *Appl. Phys. Lett.,* **101**, 132106 (2012).
53. S. Oh, G. Yang, and J. Kim, *ECS J. Solid State Sci. Technol.,* **6**, Q3022 (2017).
54. S. Ahn, F. Ren, L. Yuan, S. J. Pearton, and A. Kuramata, *ECS J. Solid State Sci. Technol.,* **6**, P68 (2017).
55. M. Higashiwaki, K. Konishi, K. Sasaki, K. Goto, K. Nomura, Q. Tu Thieu, R. Togashi, H. Murakami, Y. Kumagai, B. Monemar, A. Koukitu, A. Kuramata, and S. Yamakoshi, *Appl. Phys. Lett.,* **108**, 133503 (2016).
56. K. Konishi, K. Goto, H. Murakami, Y. Kumagai, A. Kuramata, S. Yamakoshi, and M. Higashiwaki, *Appl. Phys. Lett.,* **110**, 103506 (2017).
57. W. Feng, X. Wang, J. Zhang, L. Wang, W. Zheng, P. Hu, W. Cao, and B. Yang, J. *Mater. Chem. C,* **2**, 3254 (2014).
58. Y. Li, T.Tokizono, M. Liao, M. Zhong, Y. Koide, I. Yamada, and J.-J. Delaunay, *Adv. Funct. Mater.,* **20**, 3972 (2010).
59. Y. Qu, Z. Wu, M. Ai, D. Guo, Y. An, H. Yang, L. Li, and W. Tang, *J. Alloys Compounds,* **680**, 247 (2016).
60. F.-P. Yu, S.-L. Ou, and D.-S. Wuu, *Opt. Mater. Express,* **5**, 1240 (2015).
61. T. Oshima, T. Okuno, and S. Fujita, *Jpn. J. Appl. Physics,* **46**, 7217 (2007).
62. S. Rafique, L. Han, and H. Zhao, *Phys. Status Solidi A,* DOI 10.1002/pssa.201700063.
63. R. Suzuki, S. Nakagomi, Y, Kokubun, N. Arai, and S. Ohira, *Appl. Phys. Lett.,* **94**, 222102 (2009).
64. T. Oshima, T. Okuno, N. Arai, N. Suzuki, S. Ohira, and S. Fujita, *Appl. Phys. Express,* **1**, 011202 (2008).
65. W.-Y. Kong, G.-A. Wu, K.-Y. Wang, T.-F. Zhang, Y.-F. Zou, D._D. Wang, and L.-B. Luo, *Adv. Mater.,* **28**, 10725 (2016).
66. C.-I. Baban, Y. Toyoda, and M. Ogita, *Jpn. J. Appl. Phys.,* **43**, 7213 (2004).
67. Y. Li, A. Trinchi, W. Wlodarski, K. Galatsis, and K. Kalantarzadeh, *Sens. Actuators B,* **93**, 431 (2003).
68. M. Fleischer, M. Seth, C.-D. Kohl, and H. Meixner, *Sens. Actuators B,* **36**, 297 (1996).
69. S. Nakagomi, K. Yokoyama, and Y. Kokubun, *J. Sens. Sens. Syst.,**3***, 231 (2014).
70. M. Fleischer, and H. Meixner, *Sens. Actuators B,* **25**, 544 (1995).
71. Z. Liu, T. Yamazaki, Y. Shen, T. Kikuta, N. Nakatani, and Y. Li, *Sens. Actuators B,* **129**, 666 (2008).
72. L. Mazeina, V. M. Bermudez, F. K. Perkins, S. P. Arnold, and S. M. Prokes, *Sens. Actuators B,* **151**, 114 (2010).
73. H. Kim, C. Jin, S. An, and C. Lee, *Ceram. Int.,* **38**, 3563 (2012).
74. T. Schwebel, M. Fleischer, and H. Meixner, *Sens. Actuators B,* **65**, 176 (2000).

75. T. Yanagida, Y. Sakat, and H. Imamura, *Chem. Lett.,* **33**, 726 (2004).
76. L. Yuliati, H. Itoh, and H. Yoshida, *Chem. Phys. Lett.,* **452**, 178 (2008).
77. H. Tsuneoka, K. Teramura, T. Shishido, and T. Tanaka, *J. Phys. Chem. C,* **114**, 8892 (2010).
78. L. Yuliati, T. Hattori, H. Itoh, and H. Yoshida, *J. Catal.,* **257**, 396 (2008).
79. K. Shimura, T. Yoshida, and H. Yoshida, *J. Phys. Chem. C,* **114**, 11466 (2010).
80. Y. Hou, L. Wu, X. Wang, Z. Ding, Z. Li, and X. Fu, *J. Catal.,* **250**, 12 (2007).
81. K. Shimamura, E.G. Villora, K. Domen, K. Yui, K. Aoki, and N. Ichinose, *Jpn. J. Appl. Physics,* **44**, L7 (2005).
82. Z.-L. Xie, R. Zhang, C.-T. Xia, X.-Q. Xiu, P. Han, B. Liu, H. Zhao, R.-L. Jiang, Y. Shi, and Y.-D. Zheng, *Chinese Phys. Lett.,* **25**, 2185 (2008).
83. S. Ito, K. Takeda, K. Nagata, H. Aoshima, K. Takehara, M. Iwaya, T. Takeuchi, S. Kamiyama, I. Akasaki, and H. Amano, *Phys. Status Solidi C,* **9**, 519 (2012).
84. E. G. Villora, K. Shimamura, K. Aoki, and K. Kitamura, *Thin Solid Films,* **500**, 209 (2006).
85. E. G. Villora, K. Shimamura, K. Kitamura, K. Aoki, and T. Ujiie, *Appl. Phys. Lett.,* **90**, 234102 (2007).
86. V. I. Nikolev, A. I. Pechnikov, V. N. Maslov, A. A. Golovatenko, V. M. Krymov, S. I. Stepanov, N. K. Zhumashev, V. E. Bougrov, and A. E. Romanov, *Mater. Phys. Mechanics,* **22**, 59 (2015).